CHEMISTRY
A EUROPEAN JOURNAL

DOI: 10.1002/chem.201000498

Site-Specific Investigation of the Steady-State Kinetics and Dynamics of the Multistep Binding of Bile Acid Molecules to a Lipid Carrier Protein

Clelia Cogliati,[a, b] Laura Ragona,*[a] Mariapina D'Onofrio,[b] Ulrich Günther,[c] Sara Whittaker,[c] Christian Ludwig,[c] Simona Tomaselli,[a] Michael Assfalg,[b] and Henriette Molinari*[b]

Abstract: The investigation of multi-site ligand–protein binding and multi-step mechanisms is highly demanding. In this work, advanced NMR methodologies such as 2D ^{1}H–^{15}N line-shape analysis, which allows a reliable investigation of ligand binding occurring on micro- to millisecond timescales, have been extended to model a two-step binding mechanism. The molecular recognition and complex uptake mechanism of two bile salt molecules by lipid carriers is an interesting example that shows that protein dynamics has the potential to modulate the macromolecule–ligand encounter. Kinetic analysis supports a conformational selection model as the initial recognition process in which the dynamics observed in the apo form is essential for ligand uptake, leading to conformations with improved access to the binding cavity. Subsequent multi-step events could be modelled, for several residues, with a two-step binding mechanism. The protein in the ligand-bound state still exhibits a conformational rearrangement that occurs on a very slow timescale, as observed for other proteins of the family. A global mechanism suggesting how bile acids access the macromolecular cavity is thus proposed.

Keywords: binding mechanisms · line-shape analysis · lipids · molecular recognition · NMR spectroscopy

Introduction

It is now recognised that bile acids are important signalling molecules that regulate a network of metabolic pathways including lipid, glucose, drug and energy metabolism,[1,2] although the specific mechanisms that couple intracellular lipid processing to biological targets and signalling pathways are not yet well understood. In recent years, a number of transport proteins expressed in the liver and intestine belonging to the intracellular lipid-binding protein family (iLBP) and specifically involved in bile acid transport have been recognised as playing central roles in driving bile flow, with complex regulation of activity and function in the nucleus, cytoplasm and membrane.

Most members of iLBPs bind a single fatty acid or retinoid molecule with relatively high affinity ($K_d < 500$ nM),[3–5] whereas proteins belonging to the bile acid binding protein (BABP) subfamily seem to bind two or more ligands with differences in ligand selectivity, binding affinity, stoichiometry and binding mechanism.[6–8] This remarkable binding behaviour has implications for biological function and could be relevant for regulating the passage of bile acids through the cytoplasm.

The investigation of multi-site ligand–protein binding and multi-step mechanisms is highly demanding and a variety of biophysical techniques have been applied to tackle this problem. New experimental approaches, provided by advances in NMR spectroscopy, have been developed based on line-shape analysis[9] and relaxation dispersion experiments[10–12] that allow a reliable and sensitive investigation of ligand-binding events occurring on micro- to millisecond timescales. In particular, the combination of these methods can be useful in the study of complex mechanisms, allowing

[a] Dr. C. Cogliati, Dr. L. Ragona, Dr. S. Tomaselli
Laboratorio NMR, ISMAC-CNR, Via Bassini 15
20133 Milano (Italy)
Fax: (+39) 0223699620
E-mail: laura.ragona@ismac.cnr.it

[b] Dr. C. Cogliati, Dr. M. D'Onofrio, Dr. M. Assfalg, Prof. H. Molinari
NMR Laboratory, Biotechnology Department, University of Verona
Strada Le Grazie 15, 37134 Verona (Italy)
Fax: (+39) 0458027929
E-mail: henriette.molinari@univr.it

[c] Prof. U. Günther, Dr. S. Whittaker, Dr. C. Ludwig
School of Cancer Sciences, University of Birmingham
Vincent Drive, Birmingham, B152TT (UK)

Supporting information for this article is available on the WWW under http://dx.doi.org/10.1002/chem.201000498.

the correlation between protein internal dynamics and function to be assessed.[13,14] However, until now, their applications have been restricted to binary systems, such as, among others, the interaction of retinol with cellular retinol-binding protein,[9] which belongs to the iLBP family described here.

Investigation of the binding mechanism that leads to the formation of ternary complexes in systems endowed with different levels of cooperativity, such as those formed by bile acid binding proteins and their lipidic ligands,[15,16] is a complex task that has been addressed, for example, through stopped-flow fluorescence kinetic measurements in the case of human and rabbit BABPs.[17,18] Herein, we report an investigation employing NMR line-shape analysis and relaxation dispersion experiments of the multi-step binding mechanisms at work in the formation of adducts between chicken liver BABP (L-BABP) and two molecules of sodium glycochenodeoxycholate (GCDA), the most abundant salt of the bile acid pool. Chicken L-BABP displays the barrel structure typical of the family, formed by two orthogonal β-sheets and a helix-loop-helix motif that defines, with flexible loops, the so-called protein "open end" delineating the entrance to the cavity that hosts lipophilic ligands. The two most extensively characterised BABPs, human ileal BABP (I-BABP)[15,19] and chicken L-BABP,[19] share the common property of binding two bile salt molecules with weak intrinsic affinities and strong positive cooperativity. A number of factors have been shown to modulate ligand binding, namely the chemistry of the ligand, the nature of the protein residues[6,20] and the presence of disulfide bridges.[21] Two forms of chicken L-BABP are known that differ by the presence of a cysteine or a threonine at position 91 of the primary sequence, which results in proteins with (L-BABP/S-S) and without (L-BABP) an intramolecular disulfide bridge, respectively. The S–S bond has been shown to play an important role in regulating site selectivity.[21] Although the ligand-binding mechanism for both L-BABP/S-S and L-BABP appears to be too complex to determine the rates of association and dissociation for all the individual steps, the overall mechanism has been addressed in thermodynamic terms for L-BABP[16] through NMR titration experiments, which have allowed the identification of a binding process characterised by high cooperativity and a low intrinsic affinity. However, the mechanism of such a molecular recognition process has still to be clarified.

In line with this, the data presented herein has allowed the distinction between two different mechanisms in response to bile acid binding, namely induced fit versus conformational selection. The analysis reported herein strongly indicates that molecular recognition is promoted by a conformational selection process in which protein dynamics facilitates access of the ligand to the cavity and is therefore essential for ligand uptake. Subsequent multi-step events could be modelled in a few instances with a two-step binding mechanism, providing information on the kinetic parameters. Finally, the data reported are consistent with the protein populating an ensemble of states even in the ligand-bound state.

Results and Discussion

The NMR isotherms for the binding of ^{15}N-GCDA to unlabelled L-BABP have previously been analysed according to a site-specific model and the estimated intrinsic (site-specific) dissociation constants were determined to be $(1.0\pm0.3)\times10^{-3}$ M for both sites with a macroscopic cooperativity factor of $(9.8\pm0.4)\times10^{3}$, which translates into a macroscopic positive cooperativity described by a Hill coefficient at half-saturation of 1.98.[16] The analysis of the self-diffusion coefficients performed for both L-BABP and L-BABP/S-S consistently afforded similar data,[21] which indicates similar binding behaviour of the two proteins.

In this study line-shape analysis of NMR signals was used to elucidate the mechanism of bile salt binding to L-BABPs. Line-shape analysis of NMR resonances can provide a direct view of the mechanisms and kinetic rates of binding events or exchange processes.[22] It has been reported[23] that this approach can also be applied to protein signals in the 2D NMR spectra of ^{15}N-labelled proteins thereby allowing kinetic information to be obtained for individual residues of the protein. In the case of protein–ligand interactions the kinetic mechanism can be studied by recording spectra at different concentrations of the binding partner. Although the experimental data often exhibit complex behaviour, it has been shown that the analysis of theoretical line-shapes derived for different simplified mechanisms allows the identification of the type of kinetic mechanism responsible for a particular behaviour under steady-state conditions.[22]

The data obtained for L-BABP/S-S, for which the presence of a disulfide bridge has been shown to play a functional role,[21] are extensively discussed in the first part of the paper. The data obtained for L-BABP, consistent with the mechanism identified for L-BABP/S-S, are summarised in the second part of the paper to provide a comparative view and highlight subtle differences among the kinetics of the binding processes of the two proteins.

Analysis of L-BABP/S-S: Thirteen ^{1}H–^{15}N HSQC spectra obtained for different protein/ligand (P/L) ratios in the range of 1:0 to 1:3.5 were analysed by employing 300 μM protein samples. The highest P/L ratio was chosen to exceed the reported 1:2 stoichiometry to ensure complete protein saturation. The 1D cross-sections of the ^{1}H and ^{15}N resonance frequencies of individual protein residues, derived from the 2D NMR spectra, provide information on the effect of binding on two adjacent nuclei throughout the entire titration. The two neighbouring nuclei should experience the same kinetic mechanism, although differential effects could arise from a lack of resolution in one dimension. Owing to resonance overlap, a detailed kinetic evaluation could only be performed for 62 residues, which are evenly distributed along the protein sequence and are thus representative of all regions of the protein.

To correctly monitor the behaviour of individual cross-peak resonances during the titration, backbone resonances of holo L-BABP/S-S complexed to GCDA at a P/L ratio of

Table 1. Grouping of the residues of L-BABP/S-S according to the binding mechanism based on the line-shape analysis.

Kinetic model	Residues
K_{ex} on apo	Y9, L23, I34, F47, V48, N60, F62, G65, A68, D69, T71, D74, G75, A85, F96, V102, K103, T110, I111, G115, L118, K123
two-step binding mechanism (**A**)	
fast/slow exchange regime (**A1**)	S3, V8, E15, A22, L23, L27, V48, D69, G87, K103, G114, V116, S122
fast-to-intermediate/slow exchange regime (**A2**)	Y14, E16, F17, A20, L21, M30, Q56, G115
parallel binding mechanism (**B**)	T5, W6, Y9, E12, I34, V38, E39, F47, T50, N60, F62, T63, G65, A68, T71, D74, G75, A85, F96, V102, T110, I111 L118, I119, K123, V125
K_{ex} on holo	T5, V8, E12, E15, A22, L27, M30, V38, E39, T50, Q56, G114, V116, S122, V125

1:3 were fully assigned on the basis of standard 3D heteronuclear experiments. The resonance assignments are reported in Table S1 of the Supporting information.

The line-shape analysis of the steady-state spectra recorded along the titration path of L-BABP/S-S reveals different behaviour, as summarised in Table 1. The first observation derived from the cross-section analysis is that some residues (Table 1), mostly distributed in the β-barrel, are characterised by a low-intensity signal for the apo form, which suggests conformational exchange before ligand addition and/or exchange with solvent (Figure 1a). However, most of these residues are involved in hydrogen bonds, as evidenced both by H/D exchange experiments[24] and by the analysis of the apo X-ray structure (PDB code: 1tvq), which suggests that the reduced intensity observed mainly arises from conformational exchange-broadening. Residues showing this type of behaviour form a continuous ridge crossing the protein from the loop between the two helices to the C strand, involving residues in the EF loop, E and D strands (Figure 1b), which suggests a possible path for correlated motions. It is therefore plausible that the observed conformational averaging provides a conformational space that favours ligand binding, that is, an equilibrium P⇄P*, with P* representing a conformation suitable for ligand uptake in the internal protein cavity.

Relaxation dispersion (RD) experiments were performed to further investigate the nature of the interconverting conformers in the absence of ligand. RD experiments detect dynamics on a similar timescale as line-shape analysis and can also provide information about high-energy conformational states with populations >0.5% in exchange with a more highly populated ground state.[25] This analysis was performed on 92 residues of apo L-BABP/S-S, free from overlap, with RD spectra recorded at 600 and 900 MHz. Sixty-eight residues required an exchange contribution R_{ex} to fully describe the transverse relaxation rates $R_{2,eff}$ observed, and dispersion profiles like those reported in Figure 2a were obtained. The kinetics of the exchange process, the populations of the exchanging states and the absolute values of chemical shift differences between ground and excited states ($|\Delta\omega|$) were extracted assuming a simple two-state exchange model. The chemical shift differences obtained from the relaxation dispersion data ($|\Delta\omega|$) range between 0.2 and 2.2 ppm. The dynamic regions are evenly distributed in the protein scaffold (Figure 2b) and map the same regions that

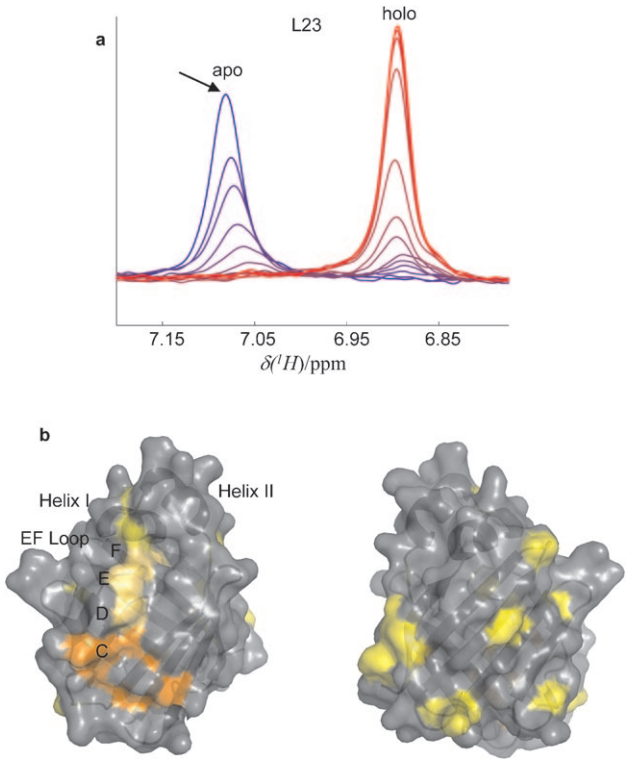

Figure 1. L-BABP/S-S residues showing a low-intensity signal for the apo form. a) ^{1}H cross-sections of ^{1}H–^{15}N HSQC titration spectra of residue L23. Experimental lines are indicated as solid lines graded from blue (apo protein) to red (holo protein) for subsequent steps in the titration. The arrow indicates the first cross-section in the absence of ligand. Note that the lines of the apo signal (at ~7.1 ppm) clearly show a shift for increasing amounts of ligand, indicative of the formation of a small amount of an intermediate in the reaction pathway. b) Residues showing a low-intensity signal for the apo form are mapped in colour on the structure. In the left panel, residues defining the ridge are colour-coded from the helical region (yellow), through the EF loop (light orange), to the C, D and E strands (orange). The right panel represents the complementary view obtained after a rotation of 180° around the z axis. No specific pattern is identified here and all residues are coloured yellow. Selected secondary structural elements are labelled.

exhibit conformational changes upon the binding of bile acid (Figure 2c), which suggests that the free protein adopts a minor conformation similar to the ligand-bound state. The chemical shift changes between the major and minor species obtained from the relaxation dispersion data potentially provide structural information on otherwise inaccessible confor-

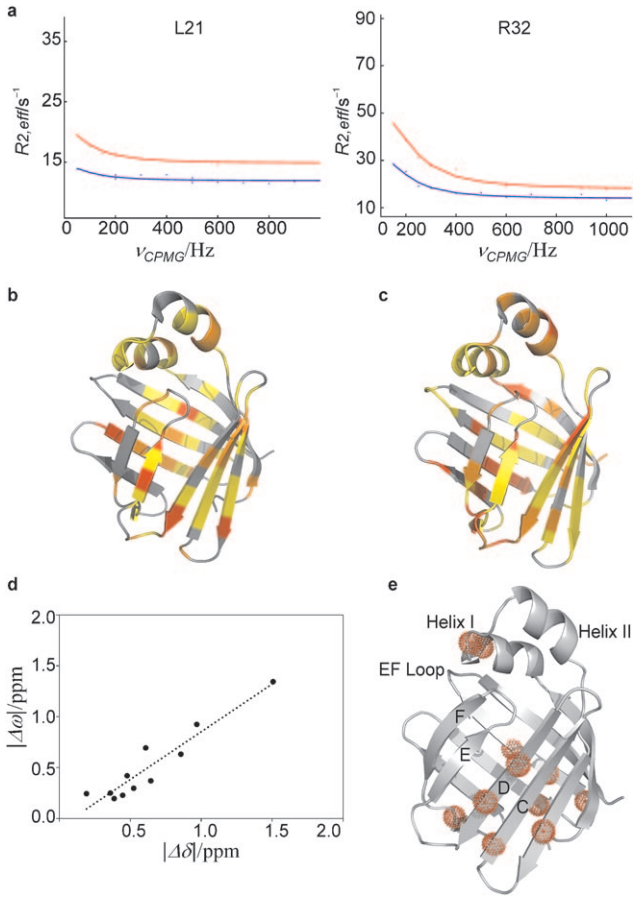

Figure 2. Comparison of chemical shift differences deduced from relaxation dispersion and titration data. a) Representative ^{15}N relaxation dispersion curves obtained for residues L21 and R32 at 600 (blue) and 900 MHz (red). b) Residues showing an exchange contribution to the backbone ^{15}N transverse relaxation rate, as observed from relaxation dispersion data, are mapped on the structure and are coloured according to their $|\Delta\omega|$ values using a scale from yellow (low values, <0.8 ppm) to red (high values, >1.5 ppm). c) ^{15}N NMR chemical shift differences between apo and holo proteins are mapped on the structure and are coloured according to their $|\Delta\delta|$ values using a scale from yellow (low values, <0.8 ppm) to red (high values, >1.5 ppm). Data are shown only for values of $|\Delta\delta|>0.2$ ppm, which is the smallest value detected from relaxation dispersion analysis. d) Linear correlation between values of $|\Delta\omega|$ and $|\Delta\delta|$ (in ppm), relative only to residues located at a distance greater than 5 Å from the two ligands (as derived from the NMR holo structure 2JN3), that is, for A20, A22, Q41, F47, T59, S61, H83, V102, E106, V108 and T110 (slope = 0.94, $R^2=0.97$). e) Residues for which the linear correlation was obtained are indicated as red dotted spheres on the structure. Selected structural elements are labelled.

mational states. Linear correlations of $|\Delta\omega|$ versus $|\Delta\delta|$, the chemical shift differences between the apo and holo states, have been interpreted as a small population of a high-energy conformation similar to the final holo state arising from the apo protein.[26] Such behaviour, when observed, is an indication that a "conformational selection" mechanism drives the ligand recognition process.

For L-BABP/S-S, in spite of a generally good qualitative agreement between the RD results ($|\Delta\omega|$) and the chemical shift differences between the apo and holo states ($|\Delta\delta|$) (Figure 2b,c), a limited quantitative agreement was observed. The observed differences were larger than the experimental uncertainties despite the good fit obtained for the RD spectra. The lack of correlation can be explained in part by the presence of direct interactions between several residues of L-BABP/S-S and the ligands that are expected to have a significant influence on the chemical shifts of the bound state. Furthermore, differences in chemical shift changes determined by RD and HSQC experiments on different states of a protein are often indicative of a more complex binding mechanism involving states with chemical shifts different to those of the apo and holo forms.[27] Thus, RD data may not be directly reconciled within the framework of the two-state exchange model employed for the fitting, for example, if there is a larger number of conformers in exchange in the apo form. Nevertheless, for a subgroup of residues not involved in any contact with the ligands in the holo protein we observe a good correlation between $|\Delta\omega|$ and $|\Delta\delta|$ (Figure 2d), as estimated by a slope of 0.94 and a correlation coefficient R^2 of 0.97. These residues are mainly located at the "open end" of the protein and in the B, C, D, F, H and I strands at the bottom of the barrel (Figure 2e). A mechanism for ligand uptake, termed the "portal hypothesis", was previously proposed in which the natural ligand enters the protein through a dynamic area, consisting of the helical region and the turns between the CD and EF strands, before binding inside the cavity.[28] The behaviour of the BABP/S-S "portal residues" is consistent with the hypothesis that the P⇄P* equilibrium involves a holo-like conformation in which the protein adopts a ligand-accessible open conformation, which supports a "conformational selection" model of binding.

A line-shape simulation was then applied, where possible, to analyse the ^1H and ^{15}N cross-sections at each titration point. The process of selecting the right model was performed as follows: in the case of slow-exchange lines, a one-step model was used only if the lines of either side were not shifted. If they were shifted an intermediate state at low abundance was applied that allows for such a shift. For the line-shapes presented, comparison with a simpler two-step mechanism with only one ligand-dependent step was also considered.[9,13,23] As this model was insufficient to describe the line-shapes, a more complex model in which both steps are ligand-dependent was constructed. Note that our model selection was always guided by reproducing features of the lines-shapes and not by reducing the numerical error between simulated and measured spectra as numerical convergence is often limited for line-shape analyses. As an example, the results obtained with a simple one-step model is reported in Figure S1. A kinetic model describing a two-step binding mechanism was then implemented in the NMRKIN software[13] for the protein complexed to two ligands (see the Experimental Section). A quantitative analysis yielding kinetic parameters and a validation of this kinetic model was feasible for a group of 21 residues (see group A, Table 1 and Figure S2). The two-step binding mechanism can be described by the general Equation (1) in which $(PL_n)^{\#}$ represents a generic intermediate that could arise from different

intermediate bound species ($n=1, 2$). Such an intermediate was generally not directly observed owing to fast exchange with the apo or holo protein and/or small populations of intermediate states. In some cases, however, the shoulders in HSQC cross-sections clearly indicate the presence of further intermediates. Simulations required that both steps were ligand-dependent, that is, $k'_{on}=k_{on}[L]$ (in which k'_{on} is the effective k_{on} rate constant), in contrast to the kinetic model employed for cellular retinol-binding protein.[9]

$$P^* + L \rightleftharpoons (PL_n)^{\#} + L \rightleftharpoons PL_2 \quad (1)$$

In the line-shape analysis, conformational exchange in the apo form, as identified by lower intensity resonances, was considered as a slow outside exchange with equilibrium constant K_{ex} ($K_{ex}<1$), as described previously.[13] This treatment is equivalent to adding an extra reaction component in slow exchange except that no chemical shift or reaction rate must be assumed for the additional reaction partner.[13] This approach should be valid in all cases in which the apo resonance is not exchange-broadened.

For all the analysed residues kinetic parameters for a two-state binding model show reasonable agreement with the experimental line-shapes, which is indicative of a binding process involving an initial fast-exchange process with an intermediate of relatively low population followed by a slower step. The first step, initiated by ligand addition, represents a lower-affinity interaction with the first ligand molecule followed by a high-affinity binding of the second ligand, consistent with an allosteric control in which the second binding event is favored by the binding of the first ligand. This could indicate that the system is endowed with some positive cooperativity, in agreement with previous results.[21]

Among the residues involved in the two-step binding mechanism, a subgroup (see group A1, Table 1) exhibits measurable chemical shift changes in the first titration steps on the side of the apo protein, typical of a fast-exchange regime ($k_{off,1}\geq 2000\ s^{-1}$), followed by a slow second step ($k_{off,2}\approx 10$–$20\ s^{-1}$). The behaviour of D69 is shown as an example in Figure 3a,c. These k_{off} rate constants point to the presence of a transient intermediate. An evaluation of the population of each species at different protein/ligand ratios was obtained from a line-shape simulation and is illustrated in Figure 3e. The derived intermediate population reaches 20% at its maximum and decays to zero with a two-fold stoichiometric amount of ligand. The residues displaying this behaviour are evenly distributed throughout the protein, consistent with the fact that they are part of an allosteric system in which binding and protein conformational changes are tightly linked.

Another subgroup of residues fitting the two-step binding mechanism (see group A2, Table 1) is characterised by a

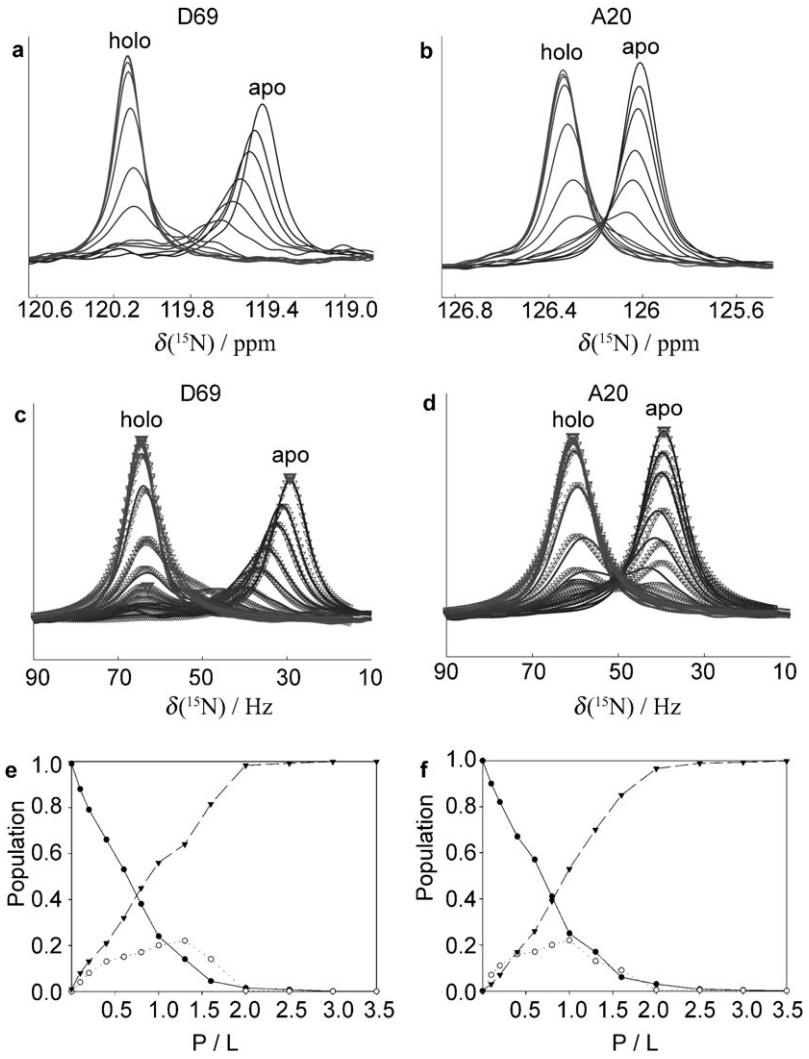

Figure 3. Line-shape simulation of L-BABP/S-S titrated with GCDA using a two-step binding mechanism [Eq. (1)]. a) ^{15}N cross-sections through ^{1}H–^{15}N HSQC titration spectra of residue D69. b) ^{15}N cross-sections through ^{1}H–^{15}N HSQC titration spectra of residue A20. Lines obtained for subsequent steps of the titration on going from the apo protein to the holo protein are shown. c,d) Line-shape simulation performed with NMRKIN for residue D69 (c) and A20 (d) (triangles). Calculated off-rates: $k_{off,1}=3000\ s^{-1}$, $k_{off,2}=10\ s^{-1}$ for D69; $k_{off,1}=500\ s^{-1}$ and $k_{off,2}=30\ s^{-1}$ for A20. e,f) Populations of species P (filled circle), I (empty circle) and PL_2 (triangle), as deduced from the line-shape analysis, are reported for residue D69 (e) and A20 (f). A colour version of the figure is given in the Supporting Information.

high-to-intermediate rate ($k_{off,1} \sim 400–600\ s^{-1}$) in the first step followed by a slow second step ($k_{off,2} \approx 10–20\ s^{-1}$; Figure 3b,d). The derived population of the intermediate state appears to be maximal (up to 20%) at a P/L ratio of around 1:1 and decays to zero with a two-fold stoichiometric amount of ligand (Figure 3f). Interestingly, mass spectrometry data recorded for different protein/ligand ratios (P/L = 1:1, 1:2, 1:5) showed the presence of a non-negligible population of protein bound to a single bile acid,[21] which suggests that the intermediate could be the singly ligated species PL_1. As all the residues characterised by the A2 type behaviour (Table 1) are localised in the portal region of the cavity (Figure 4) we suggest that whenever a singly ligated

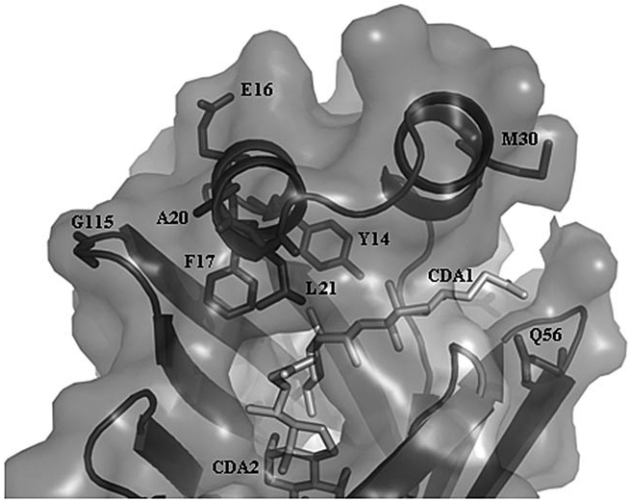

Figure 4. Mapping of residues characterised by a high-to-intermediate k_{off} rate constant in the first binding step [Eq. (1)]. Side-chains of residues Y14, E16, F17, A20, L21, M30, Q56 and G115 are shown as sticks and are labelled on the surface of L-BABP/S-S in the complex with two bile salt molecules. The two ligands are depicted in light grey and labelled as CDA1 (superficial ligand) and CDA2 (internal ligand).

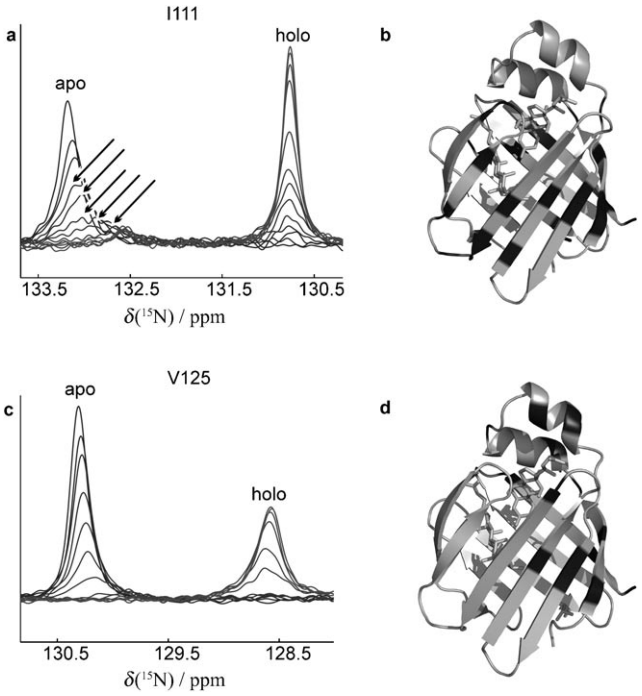

Figure 5. Residues characterised by conformational averaging. a) I111 ^{15}N cross-section exhibiting several shoulders, indicated by arrows, in intermediate titration steps. Lines obtained for subsequent steps of the titration on going from the apo protein to the holo protein are shown. b) Residues showing line-shapes with shoulders after the addition of the ligand (T5, W6, Y9, E12, I34, V38, E39, F47, T50, N60, F62, T63, G65, A68, T71, D74, G75, A85, F96, V102, T110, I111, L118, I119, K123 and V125) are labelled in dark grey on the holo L-BABP/S-S complex. c) V125 ^{15}N cross-sections exhibiting low intensity signals for the holo form. Lines obtained for subsequent steps of the titration on going from the apo protein to the holo protein are shown. d) Residues exhibiting low intensity signals in the holo form (T5, V8, E12, E15, A22, L27, M30, V38, E39, T50, Q56, G114, V116, S122 are V125) are labelled in dark grey on the holo L-BABP/S-S complex. A colour version of the figure is given in the Supporting Information.

complex is formed the bile acid binds to the superficial site. We have no evidence as to whether this equilibrium is part of a productive binding mechanism or represents an off-path intermediate. However, the identification of a singly ligated species in which the ligand preferentially occupies the superficial site is consistent with the finding that in zebrafish liver BABP, the only reported protein of the family exhibiting a 1:1 stoichiometry, the ligand binds at a superficial site located in the portal region.[29]

A large number of residues (see group B, Table 1 and Figure S2) are characterised by complex line-shapes showing many shoulders (Figure 5a). These residues are distributed throughout the β-barrel region of the protein structure (Figure 5b). Although the complexity of such line-shapes is beyond the scope of simulations, the observation that ligand addition causes shoulders that cause the apo signal to gradually disappear has previously been associated with the presence of slowly exchanging conformers as described by Scheme 1.

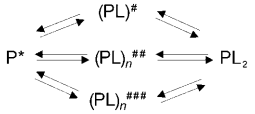

Scheme 1. Parallel binding mechanisms proposed on the basis of complex line-shapes.

Here the heterogeneity in the intermediate state (PL_n with $n = 1, 2$) can only arise from different apo states, all of which bind the ligand. In particular, this holds for all those cases in which the signal with shoulders also shifts upon ligand addition (Figure 3a). Shifting signals associated with pseudo-slow-exchange line-shapes are also a clear indication of a low population of the intermediate.[13] Binding heterogeneity is also reflected in the $^{1}H–^{15}N$ HSQC spectra of isotopically labelled GCDA bound to unlabelled protein at different P/L ratios, in which multiple resonances are detected for the ligand bound at both sites.[21]

The cross-sections of a few residues (Table 1 and Figure S2) show a holo resonance with a lower intensity than the apo signal (Figure 5c), which suggests the presence of a

slow-to-intermediate exchange between different holo species. Most of the residues that display this behaviour cluster in the two helices and in the A, B, C and J strands (Figure 5d). This pattern points to a modulation in the protein dynamics after ligand binding, which is consistent with the onset of the equilibrium $PL_2 \rightleftarrows (PL_2)^*$. As previously described for the conformational equilibria of the apo form, the onset of a similar equilibrium for the holo protein was taken into account in the simulation by using an external K_{ex} value >1 for those residues in which the signal intensity was lower in the holo form. This final protein rearrangement, relevant for binding affinity, may occur on a very slow timescale, as previously suggested for human ileal BABP.[18] Interestingly, for one residue (V116) it was possible to detect two holo forms exhibiting a measurable chemical shift difference of 20 Hz between the two holo resonances, which corresponds to an upper limit of 125 s^{-1} for the interconversion between PL_2 and $(PL_2)^*$ (Figure S3). Relaxation dispersion experiments performed on the holo protein did not show a dispersive behaviour for any residue, which indicates that conformational rearrangement should indeed occur on a slow timescale, that is, in the order of seconds.

Analysis of L-BABP: The same line-shape analysis was performed, for comparison, on L-BABP (devoid of the disulfide bridge), for which 42 residues could be analysed. The results were in complete agreement with the mechanism proposed for L-BABP/S-S. In L-BABP an intermediate exchange regime characterises the interconversion between apo conformers, as revealed by the presence of a high number of residues displaying signals with lower intensity (see Table 2 and Figure S2). Residues exhibiting an apparent slow-exchange regime could not be simulated by employing a one-step binding model, which suggests the presence of an intermediate. The line-shapes of many residues (see group A, Table 2 and Figure S2) located in helical regions and in the barrel have been fitted with a two-step binding model, as observed for L-BABP/S-S. A subgroup of residues (see group A2, Table 2) is characterised by low k_{off} rate constants for both steps ($k_{off,1}$ in the range of 20–60 s^{-1} and $k_{off,2}$ in the range of 10–20 s^{-1}) whereas another subgroup (see group A1, Table 2) is characterised by a first step with a high or high-to-intermediate rate constant ($k_{off,1} \sim 100$–$2000\ s^{-1}$) followed by a slow second step ($k_{off,2} \sim 10$–$20\ s^{-1}$). In general, L-BABP exhibits lower $k_{off,1}$ rate constants than L-BABP/S-S, which suggests a higher affinity of L-BABP for GCDA. As an example, line-shape simulations for residue S122 are reported in Figure 6a,b. Many residues, evenly distributed in the protein scaffold (Figure S4), exhibit signal intensities very similar to those of the final holo state around a molar ratio of 1:1.6 P/L (Figure 6). This observation is consistent with an allosteric behaviour and correlates with the high-binding cooperativity reported for this protein.[16]

At variance with L-BABP/S-S, the intermediate species formed along the binding pathway in L-BABP are, most likely, interconverting doubly ligated forms. Indeed, mass spectrometry experiments did not show the presence of singly ligated species at any P/L ratio below 1:2. The ^1H–^{15}N HSQC spectra of the protein recorded during the titration with the ligand support the presence of these intermediates.

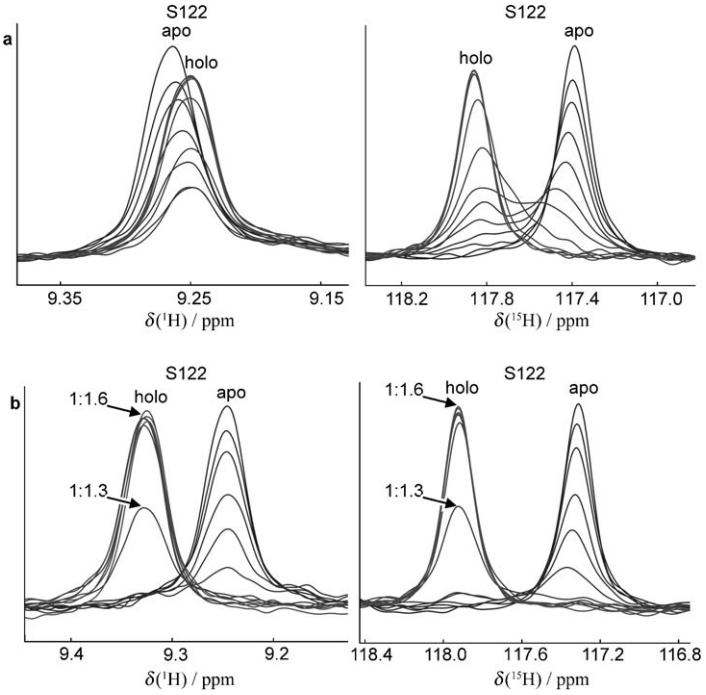

Figure 6. ^1H and ^{15}N cross-sections through the S122 cross-peak for subsequent steps of the titration of L-BABP/S-S (upper panel) and L-BABP (lower panel) with GCDA. Experimental line-shapes obtained for subsequent steps of the titration on going from the apo protein to the holo protein are shown. a) ^1H and ^{15}N cross-sections through residue S122 in the L-BABP/S-S protein. Calculated off-rates: $k_{off,1} = 3000\ s^{-1}$ and $k_{off,2} = 15\ s^{-1}$. b) ^1H and ^{15}N cross-sections through residue S122 in L-BABP. Calculated off-rates: $k_{off,1} = 100\ s^{-1}$ and $k_{off,2} = 10\ s^{-1}$. In b) the line-shapes corresponding to P/L ratios of 1:1.3 and 1:1.6 are labelled. A colour version of the figure is given in the Supporting Information.

Table 2. Grouping of residues of L-BABP according to the binding mechanism based on the line-shape analysis.

Kinetic model	Residues
K_{ex} on apo	Q7, N13, F17, L21, T63, G65, A68, G75, K79, A85, L89, T112, G115, V116, L118, I119
two-step binding mechanism (**A**)	
fast/fast-to-intermediate/slow exchange regime (**A1**)	G4, L23, E25, L27, M30, S61, K103, L118
slow/slow exchange regime (**A2**)	Q7, V8, N13, E15, F17, A20, L21, V38, Q56, T112, G114, G115, V116, S122
parallel binding mechanism (**B**)	W6, E39, I40, F47, T50, T63, G65, A68, G75, K79, A85, T112, I119, V125
K_{ex} on Holo	V8, A20, L27, M30, K35, V38, I40, F47, S51, Q56, V116, V125

In fact, in some cases the cross-peak positions reveal a curve for increasing ligand concentrations instead of a straight line between the apo and holo cross-peaks (Figure 7). This behaviour is only possible if low-population intermediates with different chemical shifts are present. Residues characterised by complex line-shapes, that is, showing small shoulders along the titration pathway, were also detected (see group B, Table 2 and Figure S2), which again suggests the presence of slow ligand binding involving intermediates. Finally, residues were detected that exhibit holo resonances of lower intensity than the corresponding apo form (Table 2 and Figure S2), consistent with the slow rearrangement $PL_2 \rightleftarrows (PL_2)^*$ (in the order of 110 s^{-1}).

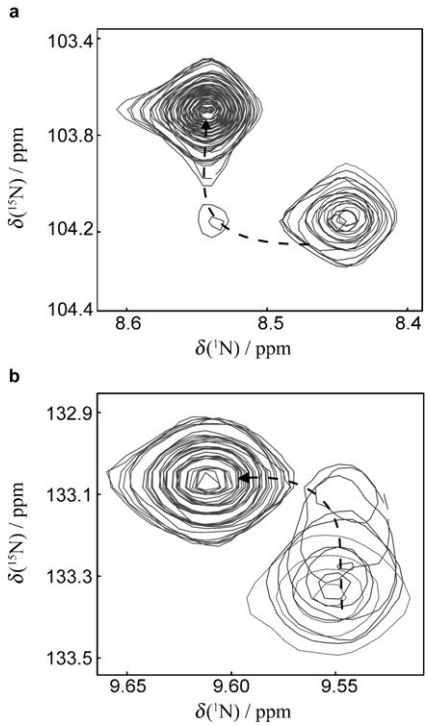

Figure 7. Superposition of the 13 ^1H–^{15}N HSQC spectra recorded for subsequent steps of the L-BABP titration with GCDA, showing cross-peaks of residue a) G115 and b) L118 moving on a "curve". The dotted arrow indicates the path followed by the peak along the titration on going from the apo to holo protein. A colour version of the figure is given in the Supporting Information.

The analysis presented allows a rationalisation of the behaviour observed for different residues in the two proteins (L-BABP/S-S and L-BABP), which contributes to the definition of the global multi-step binding mechanism presented in Equation (2):

$$P \rightleftharpoons P^* + L \rightleftharpoons (PL_n)^{\#} + L \rightleftharpoons PL_2 \rightleftharpoons (PL_2)^* \quad \text{with } n = 1,2 \tag{2}$$

These results also suggest that the presence/absence of a disulfide bridge in L-BABPs does not affect the general binding mechanism, rather it influences the kinetics of the first exchange process. The observed behaviour translates, in the case of L-BABP/S-S, into a less cooperative but site-selective system for glycochenodeoxycholic and glycocholic salts.[21] L-BABP does not display any site-selectivity, but is an extremely cooperative system.[16] Thus, the different behaviour of the two proteins may be related to the binding capability of the bile acid.

In intracellular proteins, disulfide bonds are generally transiently formed owing to the reducing nature of the cellular environment. It is plausible that an equilibrium between the oxidised and reduced forms of the L-BABPs responds to different needs for ligand uptake.

Comparison of the present results with related systems: The combination of dynamic data derived for a lipid carrier from line-shape analysis and relaxation dispersion has facilitated the distinction between two fundamentally different mechanisms in response to bile acid binding, namely, induced fit versus conformational selection. The data presented herein support the conformational selection model for liver BABPs in which the apo protein samples adopts both non-competent and competent binding conformations. Despite the complexity of a ternary complex, the mechanism involved in the binding of two ligands could be investigated to provide an estimate of the kinetics involved.

The binding mechanism for proteins belonging to the iLBP family has been addressed for human[18] and rabbit ileal-BABPs,[30] FABPs[31] and cellular retinol-binding protein (CRBP)[9] by employing stopped-flow fluorescence analysis, calorimetry and, in the case of CRBP, NMR line-shape analysis. It is therefore interesting to compare the results described herein with those reported in the literature. As already pointed out, CRBP and I-FABP bind a single ligand molecule, in contrast to the BABPs, which form ternary complexes. The detailed NMR line-shape analysis performed on CRBP reveals that site-specific mobility can be modulated by the ligand to facilitate high-affinity binding. In the model proposed, an exchange process involving a P* intermediate occurring on the millisecond timescale is sequentially followed by a slow binding step occurring on the subsecond timescale, which indicates that the encounter with the ligand "freezes" the motion of the residues located in the protein portal area.[9]

I-FABP exists as a conformation ensemble in solution in the apo form and a localised region of backbone disorder is part of the flexible portal that permits the entry of the ligand.[32] Fatty acid binding was reported to shift the order–disorder equilibrium towards the ordered closed state by stabilising a series of interactions between helix-II and the loops defining the portal area. More generally, it has been reported that solution structures of apo FABPs reveal specific regions of disorder in the portal domain, in contrast to holo FABP structures,[3,32,33] which underlies the role of conformational changes in driving the ligand protein recognition.

The kinetic data reported for human ileal BABP (hI-BABP) fitted best a reversible four-step model characterised

by a conformational change on the millisecond timescale, identified as an opening step, followed by sequential ligand binding and finally a slow conformational change on the timescale of seconds, which has been suggested to be correlated to the observed cooperativity. In the case of rabbit ileal BABP, a kinetic scheme consistent with that proposed for hI-BABP was suggested, with the only difference that the first conformational change was not observed.

When the kinetic data reported for L-BABP/S-S are compared with those reported for hI-BABP it appears that our second binding event is characterised by a lower k_{off} (~10–20 s^{-1}), to be compared with about 500 s^{-1} for hI-BABP, which suggests that binding cooperativity in L-BABPs does not rely on the last slow conformational change of the fully loaded protein, reported to be determinant for the high cooperativity of hI-BABP.[18]

Interestingly, all the described systems, with the exception of rabbit ileal BABP, are characterised by an initial conformational averaging on the millisecond timescale, possibly leading to a protein conformation competent for binding. The relaxation dispersion experiments reported herein for L-BABP provide direct evidence of a mechanism that could be a common feature of the mentioned proteins. The relevance of our results to the understanding of general rules at work in this protein family is derived, in our opinion, from the data referring to another protein of the family, namely FABP4.

In a study aimed at elucidating the nucleocytoplasmic transport of FABP4,[34] it was shown that this protein does not harbour a readily identifiable nuclear localisation signal (NLS) nor a nuclear export signal (NES) in the primary sequence. However, such signals could be found in the three-dimensional structure of the protein and were assigned to three basic residues, located in the helical region, that form a functional NLS and to three non-adjacent leucine residues, located in the antiportal region, that form a motif reminiscent of an established NES. Studies of the subcellular localisation of FABP4 support the validity of the conformational selection model for the ligand-controlled activation of the nuclear import of FABP4. It was shown in fact that upon inhibition of its nuclear export, either by blocking the export machinery or by mutating the protein's NES, a large fraction of FABP4 accumulates in the nucleus even in the absence of ligand. Hence, an import-competent conformation must exist in the apo-FABP4 population that enables the protein to enter the nucleus in the absence of ligand. These observations thus provide the first demonstration of the validity of the selection conformation model in the whole cell in a protein belonging to the same iLBP. Interestingly, L-BABP shares the same residues at both the portal and antiportal region, previously recognised as NLS and NES signals in FABP4. Thus, our model points to the relevance of the described mechanism for biological activity.

Conclusion

We have used advanced NMR methodologies, such as 2D ^{1}H–^{15}N line-shape analysis, which allows a reliable investigation of ligand binding occurring on micro- to millisecond timescales, to model a two-step binding mechanism. We have used these methods to investigate the molecular recognition and complex uptake mechanism of two bile salt molecules by lipid carriers to show that protein dynamics has the potential to modulate the macromolecule–ligand encounter. Kinetic analysis supports a conformational selection model as the initial recognition process in which the dynamics observed in the apo form is essential for ligand uptake, leading to conformations with improved access to the binding cavity. Subsequent multi-step events were modelled, for several residues, with a two-step binding mechanism. The protein in the ligand-bound state still exhibits a conformational rearrangement that occurs on a very slow timescale, as observed for other proteins of the family.

Experimental Section

Sample preparation: The proteins were expressed as previously reported.[8,21] All the protein preparations were checked by 1D ^{1}H NMR spectroscopy prior to and after delipidation, and reproducible spectra were always obtained for the apo and undelipidated forms. The molecular weights of the two proteins and the extent of the labelling was verified by MALDI mass spectrometry. All NMR samples contained 300 μM ^{15}N-BABP protein dissolved in 30 mM phosphate (Na_2HPO_4/NaH_2PO_4) and 90% H_2O/10% D_2O. The pH of the solutions was 7.2. Protein stock solution concentrations were determined by UV spectroscopy. Bile salts were purchased from Sigma. The concentrations of the ligand stock solutions were determined by measuring dry weights using a microbalance. The ligands were dissolved in the same 30 mM phosphate buffer (pH 7.2). For protein/ligand titration experiments, glycochenodeoxycholate was added to the protein in small amounts to achieve saturation within 10 steps (P/L ratios: 1:0, 0.1, 0.2, 0.4, 0.6, 0.8, 1.0, 1.3, 1.6, 2.0) and three additional aliquots were then added to ensure the end of titration (P/L ratios: 1:2.5, 3.0, 3.5).

NMR assignments: NMR spectra were acquired at 298 K on Bruker DMX 500 and Avance III 600 spectrometers equipped with a 5 mm TCI cryoprobe and Z-field gradient. Data were processed with NMRPipe[35] and visualised using NMRView.[36] For resonance assignment of L-BABP/S-S complexed with GCDA ^{1}H–^{15}N 3D TOCSY and NOESY HSQC spectra were collected. Standard pulse sequence schemes using pulsed-field gradients were employed to suppress the solvent signal and spectral artefacts. ^{1}H NMR chemical shifts were referenced to external 3-(trimethylsilyl)[3,3,2,2-D_4]propionic acid and nitrogen chemical shifts were referenced indirectly as described.[37]

The ^{1}H and ^{15}N NMR protein resonance assignments are reported in Table S1 of the Supporting information.

Line-shape analysis: For line-shape analysis spectra were recorded on a Bruker AVANCE 500 MHz spectrometer equipped with a cryogenically cooled 5 mm TXI probe. The operating field was chosen to keep the exchange in a faster regime than it would otherwise be at higher field strengths. After each ligand addition, a high-resolution sensitivity-enhanced $^{1}H/^{15}N$ HSQC spectrum was recorded with 2048 × 800 data points. Spectra were processed with zero-filling and sine window functions.

For residues that were not subject to chemical shift degeneracy, cross-sections in both spectral dimensions were extracted from all the spectra by carefully selecting slices containing the signal maxima. NMRLab software[38] was employed for spectra processing. The line-shapes for both di-

mensions were simulated simultaneously for selected kinetic models by using the set of 13 experimental spectra. NMRKIN[13] was used to calculate the time-domain signal for sections of HSQC spectra for a given kinetic mechanism assuming steady-state line-shapes as described by the equations of Gutowsky and McConnell.[39,40] The chemical shifts of signals, line-widths, populations and kinetic rate constants were adjusted iteratively to achieve consistency with experimental data. In the slow-exchange regime, only an upper limit of the off-rate can be assigned because the line-shapes depend only slightly on the rate. Residues were assigned to the model that best described their line-shapes.

Kinetic model implemented in the NMRKIN software for line-shape simulations: The line-shapes were simulated as described in the original NMRKIN publication.[13] For the case of a two-step binding mechanism, an additional model was implemented, which is described below. As described in ref. [13] the total magnetisation is obtained by summing the individual components according to Equation (3) in which $A = 2\pi i(I\nu - W_o) + R_2 + K$ in which I is the unity matrix, ν is a variable frequency defining the frequency range, W_0 is a diagonal matrix with Larmor frequencies ω, P is a column vector with the populations of the individual states, R_2 is a diagonal matrix with transverse relaxation rates $R = 1/T_2^* = \pi LW$ (line width at half height), K is a matrix containing the rate constants (rate matrix). NMRKIN calculates line-shapes in the time domain according to Equation (4), followed by the Fourier transformation to obtain the spectrum.

$$M_{tot} = I^T M = iC1^T A^{-1} P \tag{3}$$

$$F(t) = I \exp[(-K + 2\pi i W_0 - R_2)t]P \tag{4}$$

The mechanism is defined by the matrix K and by associations between rates and populations. For the simulations in this work we implemented a mechanism for two-step binding, as described by Equation (5) in which the ligand is bound in two subsequent steps. We assume that there is no direct conversion of free protein P into the product with two ligands PL_2, that is, the rates k_{13} and k_{31} have a value of zero.

$$P + L \underset{k_{21}}{\overset{k_{12}}{\rightleftharpoons}} PL_n + L \underset{k_{32}}{\overset{k_{23}}{\rightleftharpoons}} PL_2 \tag{5}$$

The rate matrix for this case is given by Equation (6). Here $k'_{12} = k_{12}[L] = \frac{1}{\tau_{12}}$ and $k'_{23} = k_{23}[L] = \frac{1}{\tau_{23}}$ depend on the concentration of ligand added.

For equilibrium conditions we obtain Equation (7) and subsequently Equation (8).

$$K = \begin{bmatrix} k'_{12} + k_{13} & -k_{21} & -k_{31} \\ -k'_{12} & k_{21} + k'_{23} & -k_{32} \\ -k_{13} & -k'_{23} & k_{31} + k_{32} \end{bmatrix} \equiv \begin{bmatrix} k'_{12} & -k_{21} & 0 \\ -k'_{12} & k_{21} + k'_{23} & -k_{32} \\ 0 & -k'_{23} & k_{32} \end{bmatrix} \tag{6}$$

$$k_{12}[L]p(P) = k_{21}p(PL_n) \tag{7}$$

$$\tau_{12} = \tau_{21}\frac{p(P)}{p(PL_n)} \tag{8}$$

For the second step of the mechanism we similarly have Equations (9) and (10).

$$k_{23}[L]p(PL_n) = k_{32}p(PL_2) \tag{9}$$

$$\tau_{23} = \tau_{32}\frac{p(PL_n)}{p(PL_2)} \tag{10}$$

After eliminating $p(PL_n)$ from Equations (8) and (10) we obtain Equation (11).

$$\tau_{21}\tau_{32}\frac{p(P)}{p(PL_2)} = \tau_{23}\tau_{12} \tag{11}$$

With $p(P) + p(PL_n) + p(PL_2) = 1$ we obtain Equation (12).

$$\tau_{23} = \tau_{32}\frac{1 - p(PL_2) - p(P)}{p(PL_2)} \tag{12}$$

The NMRKIN mechanism file was set up with these simplifications.

^{15}N relaxation dispersion: Experiments were performed on Varian Inova spectrometers equipped with room-temperature probe heads at two static magnetic fields corresponding to proton Larmor frequencies of 600 and 900 MHz. Relaxation compensated CPMG experiments were employed, performed in a constant time manner.[41] Spectra were collected as a series of 12 two-dimensional spectra with CPMG field strengths ν_{CPMG} of 50, 100, 150, 200, 300, 400, 500, 600, 700, 800, 900 and 1000 Hz with repeat experiments recorded at field strengths of 200 and 500 Hz. Eight scans were recorded per FID with a 3 s recycle time. The constant time period was set to 40 ms; the reference experiment was performed by omitting the CPMG period. Spectra were acquired with at least 1024/2 = 512 complex points for 600 MHz data and 1210/2 = 605 complex points for 900 MHz data in the F_2 dimension, respectively, whereas 128 complex points were acquired in the F_1 dimension at both magnetic field strengths. Processing and analysis of the NMR spectra were performed by employing NMRlab software.[38]

For varying the echo times, relaxation dispersion curves were obtained that depend on the chemical shift differences ($\Delta\omega$), the population of the two states and the exchange rate k_{ex}. Exchange rates (k_{ex}) were determined by fitting relaxation dispersion curves to the general expression for the phenomenological transverse relaxation rate constant in the case of two-site exchange.[23] R_{ex} was calculated from simulated parameters as described.[42] Figure S5 reports a comparison of residues showing a significant change in chemical shifts upon binding and R_{ex} contributions in the apo form.

Pymol (DeLano, W.L. The PyMOL Molecular Graphics System, DeLano Scientific, Palo Alto, CA, USA) was used for graphical representation of the results using the 1tvq and 2jn3 structures from the Protein Data Bank.

Acknowledgements

The authors are indebted to Lucia Zetta for useful discussions. This research was possible thanks to the University of Verona for financial support in the acquisition of the NMR Bruker Avance 600 MHz spectrometer and to the Cariverona Foundation for the acquisition of the cryoprobe. We acknowledge access to instrumentation at HWB NMR (University of Birmingham) supported by EU-NMR (RII3-026145). L.R. thanks the CNR-RSTL 2007 (Code No. 779) and the Italian Ministry of Health (GR2007) for financial support. C.C. was supported by a short-term fellowship from EMBO (ref. ASTF 41–2009) and by CNR short-term mobility 2008.

[1] S. M. Houten, M. Watanabe, J. Auwerx, *Embo J.* **2006**, *25*, 1419–1425.
[2] C. Thomas, R. Pellicciari, M. Pruzanski, J. Auwerx, K. Schoonjans, *Nat. Rev. Drug Discovery* **2008**, *7*, 678–693.
[3] G. V. Richieri, R. T. Ogata, A. W. Zimmerman, J. H. Veerkamp, A. M. Kleinfeld, *Biochemistry* **2000**, *39*, 7197–7204.
[4] T. Hanhoff, C. Lucke, F. Spener, *Mol. Cell. Biochem.* **2002**, *239*, 45–54.
[5] A. Chmurzynska, *J. Appl. Genet.* **2006**, *47*, 39–48.
[6] O. Toke, J. D. Monsey, G. T. DeKoster, G. P. Tochtrop, C. Tang, D. P. Cistola, *Biochemistry* **2006**, *45*, 727–737.
[7] G. P. Tochtrop, G. T. DeKoster, D. F. Covey, D. P. Cistola, *J. Am. Chem. Soc.* **2004**, *126*, 11024–11029.

[8] L. Ragona, M. Catalano, M. Luppi, D. Cicero, T. Eliseo, J. Foote, F. Fogolari, L. Zetta, H. Molinari, *J. Biol. Chem.* **2005**, *281*, 9697–9709.
[9] T. Mittag, L. Franzoni, D. Cavazzini, B. Schaffhausen, G. L. Rossi, U. L. Gunther, *J. Am. Chem. Soc.* **2006**, *128*, 9844–9848.
[10] W. Labeikovsky, E. Z. Eisenmesser, D. A. Bosco, D. Kern, *J. Mol. Biol.* **2007**, *367*, 1370–1381.
[11] J. Lipchock, J. P. Loria, *J. Biomol. NMR* **2009**, *45*, 73–84.
[12] P. Vallurupalli, D. F. Hansen, L. E. Kay, *Proc. Natl. Acad. Sci. USA* **2008**, *105*, 11766–11771.
[13] U. L. Günther, B. Schaffhausen, *J. Biomol. NMR* **2002**, *22*, 201–209.
[14] D. Kern, E. Z. Eisenmesser, M. Wolf-Watz, *Methods Enzymol.* **2005**, *394*, 507–524.
[15] G. P. Tochtrop, K. Richter, C. Tang, J. J. Toner, D. F. Covey, D. P. Cistola, *Proc. Natl. Acad. Sci. USA* **2002**, *99*, 1847–1852.
[16] M. Pedò, M. D'Onofrio, P. Ferranti, H. Molinari, M. Assfalg, *Proteins Struct. Funct. Bioinf.* **2009**, *77*, 718–731.
[17] A. M. Rea, V. Thurston, M. S. Searle, *Biochemistry* **2009**, *48*, 7556–7564.
[18] O. Toke, J. D. Monsey, D. P. Cistola, *Biochemistry* **2007**, *46*, 5427–5436.
[19] T. Eliseo, L. Ragona, M. Catalano, M. Assfalg, M. Paci, L. Zetta, H. Molinari, D. O. Cicero, *Biochemistry* **2007**, *46*, 12557–12567.
[20] G. P. Tochtrop, J. L. Bruns, C. Tang, D. F. Covey, D. P. Cistola, *Biochemistry* **2003**, *42*, 11561–11567.
[21] C. Cogliati, S. Tomaselli, M. Assfalg, M. Pedo, P. Ferranti, L. Zetta, H. Molinari, L. Ragona, *Febs J.* **2009**, *276*, 6011–6023.
[22] T. Mittag, B. Schaffhausen, U. L. Gunther, *J. Am. Chem. Soc.* **2004**, *126*, 9017–9023.
[23] T. Mittag, B. Schaffhausen, U. L. Gunther, *Biochemistry* **2003**, *42*, 11128–11136.
[24] M. D'Onofrio, L. Ragona, D. Fessas, M. Signorelli, R. Ugolini, M. Pedo, M. Assfalg, H. Molinari, *Arch. Biochem. Biophys.* **2009**, *481*, 21–29.
[25] T. Mittag, S. Orlicky, W. Y. Choy, X. Tang, H. Lin, F. Sicheri, L. E. Kay, M. Tyers, J. D. Forman-Kay, *Proc. Natl. Acad. Sci. USA* **2008**, *105*, 17772–17777.
[26] D. D. Boehr, D. McElheny, H. J. Dyson, P. E. Wright, *Science* **2006**, *313*, 1638–1642.
[27] U. Brath, M. Akke, *J. Mol. Biol.* **2009**, *387*, 233–244.
[28] A. E. Jenkins, J. A. Hockenberry, T. Nguyen, D. A. Bernlohr, *Biochemistry* **2002**, *41*, 2022–2027.
[29] S. Capaldi, M. Guariento, G. Saccomani, D. Fessas, M. Perduca, H. L. Monaco, *J. Biol. Chem.* **2007**, *282*, 31008–31018.
[30] N. Kouvatsos, V. Thurston, K. Ball, N. J. Oldham, N. R. Thomas, M. S. Searle, *J. Mol. Biol.* **2007**, *371*, 1365–1377.
[31] M. E. Hodsdon, C. Frieden, *Biochemistry* **2001**, *40*, 732–742.
[32] J. Storch, L. McDermott, *J. Lipid Res.* **2008**, *50*, 126–131.
[33] Y. He, X. Yang, H. Wang, R. Estephan, F. Francis, S. Kodukula, J. Storch, R. E. Stark, *Biochemistry* **2007**, *46*, 12543–12556.
[34] R. E. Gillilan, S. D. Ayers, N. Noy, *J. Mol. Biol.* **2007**, *372*, 1246–1260.
[35] F. Delaglio, S. Grzesiek, G. W. Vuister, G. Zhu, J. Pfeifer, A. Bax, *J. Biomol. NMR* **1995**, *6*, 277–293.
[36] B. A. Johnson, *Methods Mol. Biol.* **2004**, *278*, 313–352.
[37] D. S. Wishart, C. G. Bigam, J. Yao, F. Abildgaard, H. J. Dyson, E. Oldfield, J. L. Markley, B. D. Sykes, *J. Biomol. NMR* **1995**, *6*, 135–140.
[38] U. L. Günther, C. Ludwig, H. Ruterjans, *J. Magn. Reson.* **2000**, *145*, 201–208.
[39] H. S. Gutowsky, D. McCall, C. Slichter, *J. Chem. Phys.* **1953**, *21*, 279–292.
[40] H. M. McConnell, *J. Chem. Phys.* **1958**, *28*, 430–431.
[41] A. G. Palmer III, C. D. Kroenke, J. P. Loria, *Methods Enzymol.* **2001**, *339*, 204–238.
[42] O. Millet, P. J. Loria, C. D. Kroenke, M. N. Pons, A. G. Palmer, *J. Am. Chem. Soc.* **2000**, *122*, 10.

Received: February 25, 2010
Revised: June 11, 2010
Published online: August 16, 2010

